ACS Chemical Neuroscience

Article

Alzheimer's Protective Cross-interaction Between Wild-type and A2T Variants Alters A#42 Dimer Structure

Payel Das, Anita R. Chacko, and Georges Belfort

ACS Chem. Neurosci., **Just Accepted Manuscript** • DOI: 10.1021/acschemneuro.6b00357 • Publication Date (Web): 07 Nov 2016

ACS Publications

ACS Chemical Neuroscience is published by the American Chemical Society. 1155 Sixteenth Street N.W., Washington, DC 20036

Alzheimer's Protective Cross-interaction Between Wild-type and A2T Variants Alters $A\beta_{42}$ Dimer Structure

Payel Das[1], Anita R. Chacko[1], Georges Belfort[2]*

[1]IBM Thomas J. Watson Research Center, Yorktown Heights, NY 10598.

[2]Howard P. Isermann Department of Chemical and Biological Engineering, and Center for Biotechnology and Interdisciplinary Studies, Rensselaer Polytechnic Institute, Troy, New York 12180-3590

ABSTRACT

Whole genome sequencing has recently revealed the protective effect of a single A2T mutation in heterozygous carriers against Alzheimer's disease (AD) and age-related cognitive decline. The impact of the protective cross-interaction between the wild-type (WT) and A2T variants on the dimer structure is therefore of high interest, as the Aβ dimers are the smallest known neurotoxic species. Toward this goal, extensive atomistic replica exchange molecular dynamics simulations of the solvated WT homo- and A2T hetero- $A\beta_{1\text{-}42}$ dimers have been performed, resulting into a total of 51 μs of sampling for each system. Weakening of a set of transient, intra-chain contacts formed between the central and C-terminal hydrophobic residues is observed in the heterodimeric system. Majority of the heterodimers with reduced interaction between central and C-terminal regions lack any significant secondary structure and display a weak inter-chain interface. Interestingly, the A2T N-terminus, particularly residue F4, is frequently engaged in tertiary and quaternary interactions with central and C-terminal hydrophobic residues in those distinct structures, leading to hydrophobic burial. This atypical involvement of the N-terminus within A2T heterodimer revealed in our simulations implies possible interference on $A\beta_{42}$ aggregation and toxic oligomer formation, which is consistent with experiments. In conclusion, the present study provides detailed structural insights onto A2T $A\beta_{42}$ heterodimer, which might provide molecular insights onto the AD protective effect of the A2T mutation in the heterozygous state.

Keywords: Alzheimer's protection, amyloid beta dimer, single mutation, intrinsically disordered peptide, N-terminus, altered binding, hydrophobic collapse, molecular dynamics, replica exchange

Introduction

Alzheimer's disease (AD) is the major form of dementia, affecting ~44 million people worldwide at present, and the number is expected to double every twenty years [1]. AD is characterized by the deposition of amyloid beta (Aβ) peptides and neurofibrillary tangles into senile plaques in the brain [1]. Aβ peptide is formed via the proteolytic cleavage of the Amyloid Precursor Protein (APP) by β and γ-secretase, resulting into either of the two major isoforms, $A\beta_{40}$ and $A\beta_{42}$ [2]. While $A\beta_{40}$ is the more abundant isoform, $A\beta_{42}$ is more aggregation-prone and toxic in nature [2].

Aβ peptide is one of the intrinsically disordered proteins (IDP) [3, 4], a class of proteins lacking an unique three-dimensional structure under physiological conditions, associated with neurodegenerative diseases [5]. The lack of well-defined structure of Aβ triggers mis-folding and self-assembly to form oligomers, protofibrils, and fibrils *en route* to the deposition of amyloid plaques. Solid-state (ss) NMR suggests parallel-stacked hairpin-like structures in both $A\beta_{40}$ and $A\beta_{42}$ fibrils. The hydrophilic N-terminus (NTR, residues 1–16) appears unstructured in those fibril structures. The two hydrophobic patches, central hydrophobic cluster or CHC (residues 17–20) and C-terminal residues 30–40 (CTR), form U-shaped conformations comprised of two intermolecular, parallel, in-register β-sheets separated by a hydrophilic turn region (residues 22-29) [6, 7]. Familial mutations that alter Aβ aggregation and toxicity mainly occur in this turn region and in the NTR. Within the NTR, a novel A2V mutation (A673V in the APP gene) was identified to be AD causative in homozygous carriers, while demonstrating a protective effect in the heterozygous carriers [8]. In a seminal study, whole-genome sequence analysis of 1,795 Icelanders revealed protective effect of an A2T mutation against AD and age-related cognitive

decline [9]. This substitution, close to the β-cleavage site of APP, has been found to cause a lowered Aβ production in several studies [9,10,11].

The effect of the protective A2T mutation on the downstream events, *i.e.* Aβ aggregation and related toxicity, has just started to emerge and the findings are sometimes controversial. Maloney *et al.* observed a reduced aggregation compared to wild-type (WT) $A\beta_{42}$ [11]. On the other hand, Benilova *et al*. found a decreased aggregation tendency of A2T $A\beta_{40}$, but not for A2T $A\beta_{42}$ [10]. In a recent study, we have shown that A2T mutation does not have a substantial effect on $A\beta_{42}$ aggregation under a non-mixing condition [12]. The same study further revealed reduction of the long term potentiation (LTP) inhibition in rat hippocampal cells in presence of A2T $A\beta_{42}$ [12, 13]. Importantly, the WT+A2T mixture that closely mimics the AD protective state demonstrates an intermediate to impaired aggregation *in vitro* [10, 11].

The effect of the A2T mutation on the structure of soluble, small Aβ oligomers is largely unknown, which are considered to be the primary pathological form [14-17]. Among those, $A\beta_{1-40/1-42}$ dimers isolated from AD brains are reported to be the smallest synaptotoxic species that can impair long-term potentiation, induce cognitive defects, and initiate defects in synaptic plasticity, learning and memory [18, 19]. Aβ dimers also serve as aggregation seeds [20, 21], ultimately leading to insoluble plaques in the cerebral cortex [22-24]. Investigating the effects of the A2T mutation on the heterodimer structure is therefore critical for obtaining a deep understanding of its protective nature. The dynamic nature of Aβ dimers resulting into structural heterogeneity makes their detailed characterization challenging, even using sophisticated experiments. Molecular dynamics (MD) simulations have been serving as an useful alternative for providing detailed insights onto the structure and binding of different Aβ species (see ref[25] and references therein), including monomer [13, 26], dimers [27-34], oligomers [35-38], protofibrils [39, 40], and fibrils [25, 26, 41-43]. In this study,

we have simulated solvated A2T heterodimer and WT homodimer systems and compared the resulting structural ensembles to assess the impact of the WT-A2T cross-interaction on the dimer structure. The conformational landscapes of the WT homo- and A2T hetero-dimeric systems were explored using extensive all-atom replica-exchange molecular dynamics (REMD) simulations in explicit water. Distinct structural features of the A2T heterodimer revealed in our simulations might offer molecular explanation to the AD protective effect of the A2T mutation in the heterozygous state.

Results and discussion

Two different peptide structures were randomly selected from an earlier REMD simulation of WT Aβ_{42} monomer [13] and placed at a 15 Å distance from each other to create the initial structure (see Model and Methods section, **Fig. 1a**). To ensure that the choice of the starting peptide structures does not affect our final results, we have plotted in **Fig. 1b** the root-mean-square distance (RMSD) from the initial peptide structure as a function of simulation time for the 310 K trajectory for both systems. RMSD value reaches of 0.75 nm around 100 ns and then slowly increases to ~1 nm around 200 ns. For rest of the simulation, RMSD steadily fluctuates around that value, confirming that our results are not biased toward any particular intramolecular conformation. We have also shown the structures of both dimers at 200 ns from the 310 K trajectory (**Fig. 1c**). One chain in the WT homodimer forms a short helix near NTR, whereas the second chain populates an anti-parallel β-hairpin formed between NTR and CHC. None of these transient structural features was present in the initial structure (**Fig. 1a**). The intra-molecular structures within the A2T heterodimer at 200 ns are also significantly different from the initial ones. A parallel β-sheet formation involving the NTR of the WT chain and the CTR of the A2T chain is noticed. **Figure 1d** shows the evolutions of the distance between the center of mass (COM) of two peptides of the 310 K replica for both systems. The inter-chain distance for both dimers reaches an average value of ≤10 Å around 200 ns simulation time.

At this point, as shown in Figure 2, the first 48 replicas populate 10-55% coil, 20-70% turn, 0-38% β-sheet and 0-13% helix, ensuring that the replicas have sampled a multitude of structures and therefore, results are not biased to any particular peptide structure. Thus, the first 200 ns of each replica was discarded as the equilibration time and the remaining 200 ns portion of the

thirteen REMD trajectories in 295-311 K temperature range was considered as the production ensemble comprised of ~50,000 conformations.

Figure 3 demonstrates the results of REMD convergence analysis, as evaluated by comparing three different structural properties calculated over the time interval of 200-300 ns and 200-400 ns. These include probability distributions of radius of gyration, Rg, of individual chain and of dimer (**Fig. 3a-b**), of number of intra-peptide CHC-CTR contacts, N_{intra}, (**Fig. 3c-d**), and residue-wise turn population (**Fig. 3e-f**). The mean Rg of individual chain is 1.16 ± 0.01 nm, whereas that for the dimer is 1.28 ± 0.01 nm for both systems. The estimated Rg value for WT dimer is consistent with what was reported in earlier simulation studies [44, 45]. The estimated $\langle N_{intra} \rangle$ for homodimer is 7.32 ± 0.4 and for heterodimer is 5.90 ± 0.3. The overall range and the major features of the Rg and N_{Intra} distributions as well as of the turn propensity per residue remain unchanged, when comparing two different time intervals. This result suggests that the both systems have reached quasi-equilibrium around 200 ns.

Shown in **Figure 4** are ensemble-averaged secondary structural populations of the two dimers. To estimate the statistical significance of the computed structural properties, the production ensemble was divided into four 50 ns long non-overlapping blocks and standard errors were calculated from the standard deviations among the block averages. Small standard errors confirm the convergence of the reported estimates. **Figure 4a** shows the overall secondary structure propensities of the dimers. For comparison, data for the WT and A2T monomers are also plotted, which was taken from previously published simulations reported in ref. [13]. No major differences in the overall secondary structure profile were observed for the analyzed ensembles. Coils and turns are found to be the prevalent secondary structural elements in all species, totaling to a ~74-79% (**Fig. 4a**), suggesting highly disordered nature. About 15-19% of β-strand and <3% α–helix

content are present in the monomers as well as dimers. The absence of any significant secondary structure within WT $A\beta_{42}$ monomer [13], as reported in earlier simulations, is consistent with recent NMR measurements [46]. The low β-strand and α-helix propensities of the WT dimer found in simulations agree well with the CD-derived values (β-strand content 12-25% and α-helix content 3-9%) of $A\beta_{42}$ early aggregation species (n≤4) at 290 K and pH 7 [24, 47, 48] and with earlier implicit solvent coarse-grained simulations [35]. These results are also in line with earlier experiments [16, 49], suggesting that the secondary structure does not change much from monomer to dimer. Residue-wise secondary structure profile of the WT homodimer (**Fig. 4b**) reveals higher β-strand propensity (≥20%) in residues 17-20 and in residues 31-40, in addition to prominent (>40%) turn propensity in residues 5-10 and 23-30. Residues 12-16 show ~20% helix population. The A2T heterodimer secondary structure profile demonstrates similar characteristics (**Fig. 4c**). To obtain a more detailed comparison, residue-wise statistically significant (i.e. values larger than the corresponding standard error) β-strand, turn, and α-helix population differences between homodimer and heterodimer are plotted in **Figure 4d**. Interestingly, β-strand character near residues 10-13, 29-30, and 38-39 becomes stronger by at least 5% in heterodimer. Also, residues 5-6, residue 14-17, and residues 33-35 in heterodimer exhibit higher turn propensity. On the other hand, residues 9-11 and 29-30 show a preference toward turn conformation in WT homodimer, while a higher β-strand propensity is noticed in residues 32-34. In summary, our simulations reveal some notable differences between the secondary structure profiles of two dimers. Of interest, the N-terminus displays higher β-strand propensity in the heterodimer.

Figure 5a illustrates the ensemble-averaged intra-molecular contact probabilities. The associated standard errors and the probability differences between two dimeric systems (homodimer – heterodimer) are plotted in **Figures 5b** and **5c**, respectively. The WT homodimer

contact map suggests that all long-range (|i-j|>8) contacts are populated with less than 30% probability, *i.e.* all such contacts are transient in nature. In addition to the mutual interaction between two termini, a set of anti-parallel contacts between residues 16-21 and 31-42 are observed. Similar sets of long-range contacts were also seen in the WT Aβ_{42} monomeric ensemble [13]. Interestingly, weakening (to a ~12% probability) of those CHC-CTR intra-chain contacts is noticed in A2T heterodimer (**Fig. 5a,** lower triangle and **Fig. 5c,** upper triangle), reminiscent of the effect of introducing A2T mutation within Aβ_{42} monomer [13]. We have further estimated the intra-molecular backbone-backbone (BB) hydrogen-bonding (H-bonding) probabilities within each dimer. As shown in **Figure 5d**, all long-range intra-molecular H-bonding interactions present within dimer are fairly weak. The ones that show at least 10% probability in WT dimer are V18/G33, F20/I31, H6/L34, and D1/A42. Further weakening of the ones between CHC and CTR is noticed in the heterodimer. Taken together, our simulations reveal transient, intra-peptide interactions involving CHC and CTR within WT homodimer, which are weakened in A2T heterodimer.

The average and standard error of the inter-chain contact probabilities are shown in **Figure 6a-b.** The upper triangle of **Figure 6a** reveals that the CTR from both chains primarily contact each other at the WT dimeric interface, which agrees well with EPR [50] and ss-NMR [16] data. Additionally, some NTR-NTR and CHC-CTR inter-chain contacts are also seen, indicating hydrophobic interactions as the primary driving factor underlying dimer formation, consistent with earlier simulations [44] and experiments [50, 51]. Higher β-strand propensity (**Fig. 4b-c**) combined with the presence of inter-chain BB H-bonds (**Fig. 6c**) in those regions suggest presence of inter-molecular β-sheets at the dimeric interface. The second mode of quaternary

interaction involving CHC and CTR becomes more robust in the heterodimer (**Fig. 6a & 6c, lower triangle)**.

We have also estimated the inter-chain binding free energy using a molecular mechanics-Poisson–Boltzmann surface area method [52] (see Model and Methods section). **Figure 7a** summarizes the average and standard deviations of all energetic components. Calculations on WT homodimer and A2T heterodimer ensembles reveal comparable inter-chain binding free energy ($\Delta G^{Binding}_{Homo}$ = -17.8 ± 28.9 kcal/mol and $\Delta G^{Binding}_{Hetero}$ = -43.4 ± 28.8 kcal/mol). Both van der Waals (vdW) and electrostatic interactions contribute favorably toward dimer formation, $\Delta G^{Binding}_{vdW}$ being the predominant contributor. This result is in consistent with earlier published reports [44]. Slightly more favorable $\Delta G^{Binding}_{elec}$ is noticed in the heterodimer (**Fig. 7a**), which is also evident from the energy distribution plot (**Fig. 7b**). Our analysis indicates that this more favorable inter-chain electrostatic energies in the heterodimer can be attributed to both H-bonding (**Fig. 6c**) and salt-bridge interactions **(Table S1)**.

To further discriminate between the homo and hetero-dimeric ensemble, we compare the potential mean force (PMF) (**Fig. 7**) as a function of (i) number of CHC-CTR intra-chain contacts, N_{intra}, and (ii) the number of inter-chain contacts encompassing CHC and CTR, N_{inter} (see Methods). The PMF plot of the WT dimer reveals four distinct highly populated regions (referred as S1-S4 regions, black squares in **Fig**. **8a**), which all together represent ≥70% of the total ensemble. S1 region corresponds to the structures with minimal CHC-CTR intra-chain contacts and a weak dimeric interface. S2 state represents dimer structures with a strong interface, but weak CHC-CTR tertiary interactions. Structures with intermediate intra- and inter-chain interaction populate the S3 region, whereas S4 dimers exhibit stronger intra-chain interaction, but lack substantial inter-peptide association. The average vdW and electrostatic

inter-peptide binding energies reported in Table S2 are consistent with these observations. A significant enhancement of the S1 population is noticed in the heterodimer (from a ~9% in WT homodimer to ~23% in A2T heterodimer, **Fig. 8b,** see also **Table S3**). At the same time, S2 and S4 structures become less frequent, while S3 population stays nearly the same in heterodimer. Figure S1 illustrating conformation sampling for individual replica confirms that all replicas sample each of these four regions (S1-S4) on the heterodimer conformational landscape.

A clustering analysis was performed on the individual S1-S4 populations to extract the representative conformations (see Simulation Model and Methods). Detailed results of clustering analysis can be found in Table S3. The representative structure of the largest cluster for each sub-population (S1-S4) is shown in **Figure 8** (for additional representative structures, see **Fig. S2**). The structural diversity of those representative conformations implies heterogeneous nature of the dimeric ensemble. We also estimated the collisional cross-section (CCS) values [53] of those representative structures (Fig. 7). The CCS values for the WT homodimer range between 900 to 1050 $Å^2$. **Figure 7b** reveals similar CCS values for representative heterodimer structures. These CCS values are in line with what has been reported for WT $A\beta_{42}$ dimer in ion mobility-mass spectrometry (IM-MS) experiment [54]. The same study suggested that such CCS values are consistent with a compact, globular dimer model. Rg values of the simulated dimeric ensemble reported in this study (see **Fig. 3a**) is also indicative of collapsed structures (with an estimated scaling exponent υ = 0.39). The ensemble-averaged aspehericity, δ [4], estimated from the principal moments of the inertia tensor of the dimer is found to be ~0.04, suggesting a spherical shape. Taken together, both dimers form compact globular structures in solution, which exhibit different characteristics in terms of the transient intra- and inter-chain association.

To characterize the molecular factors resulting into enhanced population of distinct structures with low CHC-CTR interaction in the heterodimeric ensemble, we analyze those structures (S1 and S2 states) in detail. The results are summarized in **Figure 9**. Interestingly, hydrophobic regions in S1 structures show considerably weak β-strand propensity with respect to the ensemble averaged value (**Fig. 9a**). Those primarily disordered structures are largely devoid of CHC-CTR tertiary contacts and consist of a weak inter-peptide interface (**Fig. 8b-c & Table S2**). At the same time, presence of strong intra- and inter-chain NTR-CTR interaction is revealed in those structures (**Fig. 8b-c**). Residues from extreme N-terminus are also found in contact with residues 18-23.

Figure 9a shows a representative S1 heterodimer structure, revealing strong participation of hydrophobic residues in those distinct NTR-CTR interactions. Typically, F4 from the NTR is found to be strongly engaged in interaction with CTR hydrophobic residues such as I32, M35, and V39 from A2T peptide, and I31 and V36 from WT peptide. T2 appears to be solvent-exposed in that state, which is further supported by the solvent-exposed surface exposure (SASA) values: 80 $Å^2$ for T2 and 60 $Å^2$ for A2. In contrast, same residues display SASA values of ~50 $Å^2$ in the S3 state. These results suggest that a solvent-exposed T2 allows formation of a buried hydrophobic cluster at the inter-chain interface, which involves residues such as F4, I31, I32, M35, and V36. Such altered interface inhibits tertiary hydrophobic interactions between CHC and CTR, as well as typical inter-peptide CTR-CTR association.

Structural differences between two dimeric systems are also noticed in the S2 state that represents strongly-bound dimers. It should be noted that S2 structures are less frequently populated in the heterodimer. S2 conformations in the homodimeric ensemble exhibit reduced CHC-CTR tertiary interaction, robust β-strand tendency around CTR, and inter-chain CHC-CTR

and CTR-CTR contacts. The extensive interface in the S2 homodimer is often comprised of CTR β-strands, arranged in parallel or anti-parallel manner (**Fig. 8a and S2**). Stronger β-strand propensity at CHC, more robust CHC-CTR tertiary interactions, and enhanced anti-parallel CHC-CTR and CTR-CTR contacts are seen in S2 heterodimers. Consistently, snapshot of the most representative S2 heterodimer structure reveals a CHC-CTR hairpin within the WT chain (**Fig. 10b,** for more structures see **Fig. S2**). CHC and CTR of the A2T chain are primarily engaged in inter-peptide contacts, resulting in anti-parallel β-sheet structure. In those structures, the NTR of the A2T chain is again found to interact with hydrophobic residues from CHC and CTR, e.g. L17, V39, V40, I41, and A42, that constitute the inter-chain interface. It seems that, weaker CHC-CTR tertiary interaction and preference of A2T NTR to interact with distant hydrophobic residues result in formation of distinct S1 and S2 heterodimer structures. (**Fig. 9-10**).

Figure 11 summarizes the structural analyses of S3 and S4 populations, in which both chains form CHC-CTR tertiary contacts with moderate to strong tendency (for representative structures, see **Fig. S2**). It should be noted again that S4 conformations are weakly populated in the heterodimeric system. Robust β-strand character near CHC and CTR is seen in those dimers (**Fig. 11a**). Consistently, a prevalence of β-hairpin conformation involving CHC and CTR emerges, particularly within S4 dimers. Some alternative modes of quaternary association are revealed, such as CHC-CHC in homodimer and NTR-CHC in heterodimer within S4 state. Additionally, higher β-strand propensity in NTR is found in S4 heterodimers (**Fig. 11d**).

Table 1 summarizes the main findings reported in the present simulation study as well as the experimental observations published till to date on the WT+A2T $A\beta_{42}$ mixture, some of which

can be explained in light of the molecular insights obtained from this study. Overall, both dimeric ensembles appear structurally heterogeneous in nature. Ensemble-averaged structural features of the WT dimer revealed in the present study, such as transient CHC-CTR tertiary interaction and inter-molecular β-sheet (both parallel and anti-parallel) at CTR, are consistent with experimental reports of Aβ oligomers [16, 55]. The simulated WT $A\beta_{42}$ dimeric landscape further demonstrates different sub-populations that vary in the involvement of central and C-terminal hydrophobic regions in intra- and inter-chain binding. An anti-correlation relationship emerges, *i.e.* intra-molecular conformations with weak CHC-CTR interactions form an extensive interface by actively interacting *via* those regions (**Fig. 8a**). In those strongly-bound WT $A\beta_{42}$ dimer structures, β-sheets encompassing CTR are often seen at the interface, whereas CHC lacks any secondary structure. In contrast, strong β-strand character is seen at both CHC and CTR in the WT homodimer structures that display intermediate to strong CHC-CTR tertiary interaction and a relatively weak interface. Presence of a β-hairpin involving CHC and CTR is also noticed in those dimers.

Notable structural differences between WT $A\beta_{42}$ homodimer and A2T $A\beta_{42}$ heterodimer are found, such as stronger β-strand character at the NTR and weaker tertiary interaction between central and C-terminal hydrophobic regions in the heterodimer. Average CHC-CTR contact probability is found to be 0.12 in heterodimer, while the same is 0.21 in the WT homodimer (**Table 1**). Consistently, conformations with robust CHC-CTR intra-chain interaction become less populated in the heterodimeic landscape. In addition, the population of strongly-bound dimers becomes smaller in the heterodimeric ensemble. Instead, distinct dimer structures (S1) with little secondary structure, weak CHC-CTR tertiary interaction, and reduced inter-chain binding are frequently visited in the heterodimeric landscape. The A2T NTR is involved in

atypical tertiary and quaternary interactions with the central and C-terminal hydrophobic regions in those distinct heterodimers, often leading to hydrophobic burial.

The observed lowering of transient β-hairpin structures (S4 state) in the simulated A2T heterodimer might provide an explanation for the protection against AD in the heterozygous carriers, as the β-hairpin structures are found to be crucial in amyloid aggregation and toxicity. We have previously reported transient β-hairpin depletion in the simulated A2T $A\beta_{42}$ monomeric ensemble, which was primarily attributed to unique electrostatic interactions between NTR and the turn region [13]. The fact that the β-hairpins present hydrophobic surfaces exposed to solvent is directly correlated with their aggregation propensity and neurotoxicity [56-58]. For instance, double-cysteine mutants ($A\beta40_{cc}$ and $A\beta42_{cc}$) with overly stable β-hairpin monomeric conformation have been reported to lower fibril formation and enhance toxic β-sheet oligomer and/or protofibril population [15]. NMR and AFM experiments have suggested presence of double-hairpin monomers within toxic $A\beta_{42}$ oligomers [16]. The explicit formation of double-hairpin structures in $A\beta_{42}$ (and not $A\beta_{40}$) has been linked to the higher aggregation propensity and toxicity of the longer isoform [59]. Therefore, formation of a transient Aβ β-hairpin monomer is thought to be the very first step of oligomerization [59,37, 60, 61]. A two-stage dock-and-lock mechanism for oligomer growth has been proposed, in which a disordered monomer adds to the oligomers containing hairpin-like structures [60].

Earlier studies have further suggested the need for stronger inter-peptide association in order to form aggregation nuclei, thus providing a connection between aggregation thermodynamics and kinetics [62]. Accordingly, a recent AFM study has shown the weaker inter-peptide interaction in $A\beta_{40}$ dimer due to the involvement of NTR. In contrast, a stronger $A\beta_{42}$ dimer interface was found with predominant contribution from CTR [63]. Such difference in inter-peptide association is

believed to be key in determining the higher aggregation propensity and neurotoxicity of $A\beta_{42}$ [64]. Therefore, weaker inter-molecular binding, combined with hydrophobic coalescence, seen in S1 heterodimers might trigger an inhibitory effect on $A\beta_{42}$ aggregation and toxicity in the WT+A2T mixture. This result is in line with the experimentally observed intermediate [11] to impaired [10] aggregation of the WT+A2T $A\beta_{42}$ mixture (Table 1). IM-MS has further revealed presence of small oligomers (such as dimers, tetramers, and hexamers), but not toxic dodecamers, in an equimolar WT + A2T $A\beta_{42}$ mixture [14]. As the toxic Aβ oligomers are believed to be β-sheet rich, the highly disordered nature of the S1 heterodimers provides a molecular explanation to the absence of toxic oligomers in mixture. The altered tertiary and quaternary packing of the simulated heterodimer is also in good agreement with the ANS binding results, indicating decreased exposed hydrophobic surface in the early WT+A2T $A\beta_{42}$ aggregates [10]. The disordered heterodimer structures are further consistent with the Fourier Transform Infrared Spectra of the WT+A2T $A\beta_{42}$ mixture suggesting presence of characteristic non-β-sheet structures [10]. Taken together, the heterodimer structure reported in this study is not only consistent with existing experimental findings, but also sheds light onto the aggregation differences reported for the WT+A2T $A\beta_{42}$ mixture.

The pivotal role of N-terminus in Aβ structure, oligomerization/aggregation, and toxicity is becoming increasingly evident [65], [66], [67]. N-terminus specific antibodies are known to effectively bind both soluble and insoluble forms of Aβ [68]. Amyloid inhibitor tetra-peptides are also known to bind at the Aβ NTR [69]. Recently, a small peptide homologous to 1-6A2V has been reported to hinder Aβ amyloidogenesis and neurotoxicity [70]. Several studies have further revealed the crucial involvement of the Aβ N-terminus in tertiary and quaternary interactions. A novel triple β-sheet motif within $A\beta_{42}$ oligomers has been experimentally reported with minimally exposed

hydrophobic residues, in which association between the NTR and residues 17-22 was revealed [71]. A simulation study by Head-Gordon and coworkers has shown typical antiparallel β−hairpin involving CHC and CTR in $A\beta_{42}$ monomer, whereas a characteristic antiparallel β−hairpin population comprising CHC and N−terminal residues 9−13 was observed in $A\beta_{40}$ monomer [72]. Simulations performed by Urbanc and coworkers [36, 45] have revealed tertiary interaction between NTR (A2-F4) and CHC residues within $A\beta_{40}$ dimer, but not in $A\beta_{42}$ dimer. A more flexible NTR might be associated with enhanced toxicity of $A\beta_{42}$ oligomers. A recent MD study of an AD protective A2V $A\beta_{40}$ heterodimer has indicated less energetically favorable inter-peptide interface, reduction of all-alpha structures, along with higher NTR-CHC intra-peptide contacts [73]. In line with these earlier studies, our simulations reveal enhanced tendency of the A2T NTR, particularly residue F4, to be engaged in atypical interaction with CHC and CTR. Such interaction often leads to structurally disordered, collapsed structures within the A2T heterodimeric ensemble that is associated with AD protection.

One attractive pharmacological strategy for AD is to design drugs that can interfere with Aβ aggregation and toxicity by binding to different Aβ species, particularly to the β-sheet rich oligomers [74]. Options include small organic molecules [75, 76], short peptides [70, 77, 78], and Aβ-interacting proteins [38, 79, 80]. Presence of aromatic and hydrophobic moieties is common in those amyloid inhibitors. Selected, short amyloid inhibitor peptides in D-isomeric form are often found to be more effective [70, 78], as they are protease-resistant. Given the importance of intra- and inter-peptide interactions involving Aβ N-terminus in modulating Aβ structure, aggregation, and toxicity, a plausible pathway toward intervention is to design inhibitory peptides composed of WT (^{1}DAEFRH^{6}) sequence or its variants [70]. The aim is to design inhibitory peptides capable of

interfering with Aβ interactions (e.g. those between CHC and CTR) leading to toxic oligomer formation.

In summary, the present simulation study reports enhanced population of primarily disordered structures within the A2T $A\beta_{42}$ heterodimeric ensemble, when compared to the WT $A\beta_{42}$ dimer. Key characteristics of those distinct heterodimer structures are overall low secondary structure content, reduced CHC-CTR tertiary interaction, and a weak inter-chain interface, The NTR is frequently engaged in tertiary and quaternary interactions with central and C-terminal hydrophobic residues in those distinct heterodimer structures. The unique heterodimer structure revealed in this study might provide molecular insights onto the protective effect of the A2T mutation in the heterozygous state. In future, we plan to investigate the further assembly and membrane association of these distinct heterodimer structures, in order to directly characterize their effect on Aβ aggregation and toxicity.

Simulation Model and Methods

In this study, we have used extensive replica exchange molecular dynamics (REMD) simulations to characterize the conformational landscape of WT homodimer and A2T heterodimer. REMD is an enhanced sampling algorithm that helps the system to escape the local minima in the free energy landscape by increasing temperature [81]. The method consists of several identical copies or replicas of the system, which are simulated in parallel over a range of temperatures. At frequent intervals, trials to exchange the temperature of all neighboring replicas are performed, according to a Metropolis Monte Carlo criterion. The swapping probability is chosen to satisfy a detailed balance. This method has been successfully applied to construct the ensemble of intrinsically disordered peptides that lack a single native conformation and instead populate multiple rapidly interchanging states, such as Aβ at atomic resolution [58, 82-84].

The following protocol was used to set up the solvated dimer systems. Two different monomeric structures were randomly selected from an earlier REMD simulation of the solvated WT $A\beta_{42}$ monomer [13], which were populated at around room temperature. The monomer structures were placed in a 74 x 74 x 74 $Å^3$ cubic box containing ~12290 water molecules, such that the minimum distance (heavy atom only considered) between two monomers was at least 15 Å (see Fig. 1a). This results in an effective concentration of 8mM. The protonation states of the acidic and basic residues of the peptides were set at pH 7. Six Na^+ ions were added to neutralize the system charge. For the A2T heterodimer, the initial system set-up was identical to that of the WT homodimer, except that the sidechain of the residue 2 of one peptide chain was mutated *in silico* to that of the threonine. The system was first energy minimized, followed by a 100 ps equilibration in NPT ensemble (300 K and 1 atm), during which the protein backbone remained constrained. Next, a 200 ps long MD simulation was performed without applying any constraint,

in order to allow the system to fully relax. The final structure at the end of this run was used as the starting structure for REMD run. Finally, constant-volume REMD runs were performed using a 2 fs time-step. A total of 128 replicas within an exponentially distributed temperature range [85] of 295-503 K were used. The replica exchange attempts were made every 4 ps. The system was coupled to a Nose-Hoover heat bath to maintain constant temperature between swaps. Use of this protocol results in an average exchange ratio of 30% that is constant over the temperature range. An aggregate simulation time of 51.2 μs per system was generated per system. To our knowledge, this is the most extensive simulation study on the $A\beta_{42}$ dimer system reported to date.

The particle-mesh Ewald (PME) method was used for the long-range electrostatic interactions [86], while the van der Waals interactions were treated with a cut-off distance of 10 Å. The bonds were constrained using LINCS [87] and SETTLE [88] algorithms. Simulations were performed using the GROMACS4.5.4 software [89]. All MD simulations were run using IBM BlueGene/Q supercomputers. For all calculations, a combination of OPLS-AA force-field [90] and TIP3P water model [91] was used. We have previously used this combination of parameters in conjunction with 64 replicas, each ~225 ns long, to generate the structural ensemble of $A\beta_{42}$ monomer [13]. The resulting ensemble was found to be in good agreement with NMR experiments [59]. A highly disordered nature of the $A\beta_{42}$ monomer was found in those simulations [13], in line with recent NMR experiments [46]. The combination of OPLS-AA and TIP3P parameters has been also found to be suitable for simulating assembly of Aβ fragments [92] and full-length Aβ peptides [34].

Simulation Analysis

Conformational analysis: The secondary structure was estimated using the STRIDE program [93]. Residue-specific secondary structural propensity was estimated by counting the percentage of conformations, in which a residue forms the secondary structure of interest. A cutoff distance of 8 Å between C_α atoms was considered to define a C_α-C_α contact between two residues. For contacts between heavy atoms, a cutoff distance of 5 Å was used. Only non-sequential contacts ($|i-j| \geq 3$) were considered for tertiary interactions. For quaternary association, only those structures were considered that have ≥ 25 contacts (heavy atom only) between two chains. Hydrogen bonds were determined with a cutoff of 3.5 Å for the donor-acceptor distance and a cutoff of 30° for the donor-hydrogen-acceptor angle. The non-polar solvation energy was calculated using the solvent accessible surface area (SASA) where a probe of 1.4 Å radius was rolled over the protein surface. Asphereicity, δ, a shape measure of polymers, was calculated from the three normalized eigenvalues (λ) of the gyration tensor. The eigenvalues denote the shape of the polymer in principal directions. Asphereicity, δ, was obtained from the equation: $\delta = \frac{(\lambda_1 - \lambda_2)^2 + (\lambda_2 - \lambda_3)^2 + (\lambda_1 - \lambda_3)^2}{2(\lambda_1 + \lambda_2 + \lambda_3)^2}$ [94]. So, if three eigenvalues are equal, δ is equal to zero and the polymer has a spherical shape. If all the eigenvalues are zero except one, then δ is equal to one and the polymer has a rod-like shape. All peptide structure figures were rendered using VMD [95]. The convergence of the simulations was checked by dividing the simulation data in two or four equal sets and estimating the standard errors or similarity of the structural features obtained from those sets.

Binding energy calculation: The average inter-chain binding free energies ($\Delta G_{Binding}$) for the homo- and hetero- dimer were calculated using the MM-PBSA method [52, 96]. Binding energy calculation by this method does not account for the entropic term. Approximately ~4000 structures comprising S1-S4 states (every 10th frame of the ensemble was considered) were taken into account for this calculation. The total binding energy is a cumulative of the molecular mechanics energy (van der Waals and electrostatics) and solvation (non-polar and polar solvation) energy terms. The non-polar solvation energy was estimated using a model based on solvent-accessible surface area calculation.

PMF analysis and clustering: Potential of mean force (PMF, W(X)) plots were obtained from a histogram analysis, using the equation $W(x) = -RT.\log(p(X))$, where X is the set of reaction coordinates and p(X) is the probability. The average number of intra-chain CHC-CTR contacts, and the total number of inter-chain contacts involving CHC and CTR were used as the reaction coordinates for PMF estimation. Since the probability of CHC-CHC mode of inter-peptide association was found to be very low, only CHC-CTR and CTR-CTR quaternary contacts were considered for PMF analysis. Regions on the PMF plots that individually represent ≥9% of total production ensemble were further analyzed. A cluster analysis using the Daura algorithm [97] was performed. A 6 Å C_α-RMSD cut-off between two conformations was used for cluster analysis of the highly populated regions on the PMF plots.

Collision cross section (CCS) calculation: Ion mobility mass spectrometry (IM-MS) provides information on the size and stoichiometry of protein assemblies. CCS values of ions are estimated by measuring the time taken for them to traverse a region of inert gas under the influence of a weak electric field [98]. We used IMPACT (Ion Mobility Projection Approximation

Calculation Tool), a fast and accurate method to calculate the CCS values of the representative dimer structures using their atomic coordinates [53].

Supporting Information (SI)

Additional figures and tables.

Acknowledgements

Support from IBM BlueGene Science Program is acknowledged by PD. GB acknowledges RPI for Institute funds from his endowed Chair.

REFERENCES

1. Selkoe, D. J. Alzheimer's disease: genes, proteins, and therapy. *Physiol Rev* 2001, 81, 741-766.
2. Klein, A. M.; Kowall, N. W.; Ferrante, R. J. Neurotoxicity and Oxidative Damage of Beta Amyloid 1–42 versus Beta Amyloid 1–40 in the Mouse Cerebral Cortex. *Ann. N. Y. Acad. Sci.* 1999, 893, 314-320.
3. Gall, T. L.; Romero, P. R.; Cortese, M. S.; Uversky, V. N.; Dunker, A. K. Intrinsic disorder in the protein data bank. *Journal of Biomolecular structure and dynamics* 2007, 24, 325-341.
4. Mao, A. H.; Lyle, N.; Pappu, R. V. Describing Sequence-Ensemble Relationships for Intrinsically Disordered Proteins. *The Biochemical journal* 2013, 449, 307-318.
5. Chiti, F.; Dobson, C. M. Protein misfolding, functional amyloid, and human disease. In *Annual Review of Biochemistry*, 2006; Vol. 75, pp 333-366.
6. Petkova, A. T.; Ishii, Y.; Balbach, J. J.; Antzutkin, O. N.; Leapman, R. D.; Delaglio, F.; Tycko, R. A structural model for Alzheimer's beta-amyloid fibrils based on experimental constraints from solid state NMR. *Proc Natl Acad Sci USA* 2002, 99, 16742-16747.
7. Luhrs, T.; Ritter, C.; Adrian, M.; Riek-Loher, D.; Bohrmann, B.; DÃ¶beli, H.; Schubert, D.; Riek, R. 3D structure of Alzheimer's amyloid-beta(1-42) fibrils. *Proc Natl Acad Sci USA* 2005, 102, 17342-17347.
8. Di Fede, G.; Catania, M.; Morbin, M.; Rossi, G.; Suardi, S.; Mazzoleni, G.; Merlin, M.; Giovagnoli, A. R.; Prioni, S.; Erbetta, A.; Falcone, C.; Gobbi, M.; Colombo, L.; Bastone, A.; Beeg, M.; Manzoni, C.; Francescucci, B.; Spagnoli, A.; CantÃ¹, L.; Del Favero, E.; Levy, E.;

Salmona, M.; Tagliavini, F. A Recessive Mutation in the APP Gene with Dominant-Negative Effect on Amyloidogenesis. *Science* 2009, 323, 1473-1477.
9. Jonsson, T.; Atwal, J. K.; Steinberg, S.; Snaedal, J.; Jonsson, P. V.; Bjornsson, S.; Stefansson, H.; Sulem, P.; Gudbjartsson, D.; Maloney, J.; Hoyte, K.; Gustafson, A.; Liu, Y.; Lu, Y.; Bhangale, T.; Graham, R. R.; Huttenlocher, J.; Bjornsdottir, G.; Andreassen, O. A.; Jonsson, E. G.; Palotie, A.; Behrens, T. W.; Magnusson, O. T.; Kong, A.; Thorsteinsdottir, U.; Watts, R. J.; Stefansson, K. A mutation in APP protects against Alzheimer's disease and age-related cognitive decline. *Nature* 2012, 488, 96-99.
10. Benilova, I.; Gallardo, R.; Ungureanu, A.-A.; Castillo Cano, V.; Snellinx, A.; Ramakers, M.; Bartic, C.; Rousseau, F.; Schymkowitz, J.; De Strooper, B. The Alzheimer Disease Protective Mutation Ala2Thr Modulates Kinetic and Thermodynamic Properties of Abeta Aggregation. *Journal of Biological Chemistry* 2014.
11. Maloney, J. A.; Bainbridge, T.; Gustafson, A.; Zhang, S.; Kyauk, R.; Steiner, P.; van der Brug, M.; Liu, Y.; Ernst, J. A.; Watts, R. J.; Atwal, J. K. Molecular Mechanisms of Alzheimer's Disease Protection by the A673T Allele of Amyloid Precursor Protein. *Journal of Biological Chemistry* 2014.
12. Murray, B.; Sorci, M.; Rosenthal, J.; Lippens, J.; Isaacson, D.; Das, P.; Fabris, D.; Li, S.; Belfort, G. A2T and A2V Aβ Peptides Exhibit Different Aggregation Kinetics, Primary Nucleation, Morphology, Structure and LTP Inhibition. *Proteins: Structure, Function, and Bioinformatics* 2016.
13. Das, P.; Murray, B.; Belfort, G. Alzheimer's Protective A2T Mutation Changes the Conformational Landscape of the Aβ1–42 Monomer Differently Than Does the A2V Mutation. *Biophysical Journal* 108, 738-747.
14. Zheng, X.; Liu, D.; Roychaudhuri, R.; Teplow, D. B.; Bowers, M. T. Amyloid β-Protein Assembly: Differential Effects of the Protective A2T Mutation and Recessive A2V Familial Alzheimer's Disease Mutation. *ACS chemical neuroscience* 2015, 6, 1732-1740.
15. Sandberg, A.; Luheshi, L. M.; Sollvander, S.; Pereira de Barros, T.; Macao, B.; Knowles, T. P. J.; Biverstal, H.; Lendel, C.; Ekholm-Petterson, F.; Dubnovitsky, A.; Lannfelt, L.; Dobson, C. M.; Hard, T. Stabilization of neurotoxic Alzheimer amyloid-beta oligomers by protein engineering. *Proceedings of the National Academy of Sciences* 2010, 107, 15595-15600.
16. Ahmed, M.; Davis, J.; Aucoin, D.; Sato, T.; Ahuja, S.; Aimoto, S.; Elliott, J. I.; Van Nostrand, W. E.; Smith, S. O. Structural conversion of neurotoxic amyloid-[beta]1-42 oligomers to fibrils. *Nat Struct Mol Biol* 2010, 17, 561-567.
17. Nguyen, P. H.; Tarus, B.; Derreumaux, P. Familial Alzheimer A2 V Mutation Reduces the Intrinsic Disorder and Completely Changes the Free Energy Landscape of the Abeta1-28 Monomer. *J Phys Chem B* 2014, 118, 501-510.
18. Shankar, G. M.; Li, S.; Mehta, T. H.; Garcia-Munoz, A.; Shepardson, N. E.; Smith, I.; Brett, F. M.; Farrell, M. A.; Rowan, M. J.; Lemere, C. A. Amyloid-β protein dimers isolated directly from Alzheimer's brains impair synaptic plasticity and memory. *Nature medicine* 2008, 14, 837-842.
19. Müller-Schiffmann, A.; Herring, A.; Abdel-Hafiz, L.; Chepkova, A. N.; Schäble, S.; Wedel, D.; Horn, A. H. C.; Sticht, H.; de Souza Silva, M. A.; Gottmann, K.; Sergeeva, O. A.; Huston, J. P.; Keyvani, K.; Korth, C. Amyloid-β dimers in the absence of plaque pathology impair learning and synaptic plasticity. *Brain* 2016, 139, 509-525.
20. Shankar, G. M.; Bloodgood, B. L.; Townsend, M.; Walsh, D. M.; Selkoe, D. J.; Sabatini, B. L. Natural Oligomers of the Alzheimer Amyloid-beta Protein Induce Reversible Synapse Loss

by Modulating an NMDA-Type Glutamate Receptor-Dependent Signaling Pathway. *J Neurosci* 2007, 27, 2866-2875.
21. Pujol-Pina, R.; Vilaprinyó-Pascual, S.; Mazzucato, R.; Arcella, A.; Vilaseca, M.; Orozco, M.; Carulla, N. SDS-PAGE analysis of Aβ oligomers is disserving research into Alzheimer´ s disease: appealing for ESI-IM-MS. *Scientific reports* 2015, 5.
22. Langer, F.; Eisele, Y. S.; Fritschi, S. K.; Staufenbiel, M.; Walker, L. C.; Jucker, M. Soluble Aβ seeds are potent inducers of cerebral β-amyloid deposition. *The Journal of neuroscience* 2011, 31, 14488-14495.
23. Taylor, B. M.; Sarver, R. W.; Fici, G.; Poorman, R. A.; Lutzke, B. S.; Molinari, A.; Kawabe, T.; Kappenman, K.; Buhl, A. E.; Epps, D. E. Spontaneous aggregation and cytotoxicity of the beta-amyloid Abeta1-40: a kinetic model. *Journal of protein chemistry* 2003, 22, 31-40.
24. Ono, K.; Condron, M. M.; Teplow, D. B. Structure-neurotoxicity relationships of amyloid beta-protein oligomers. *Proc Natl Acad Sci USA* 2009, 106, 14745-14750.
25. Nasica-Labouze, J.; Nguyen, P. H.; Sterpone, F.; Berthoumieu, O.; Buchete, N.-V.; Coté, S.; De Simone, A.; Doig, A. J.; Faller, P.; Garcia, A.; Laio, A.; Li, M. S.; Melchionna, S.; Mousseau, N.; Mu, Y.; Paravastu, A.; Pasquali, S.; Rosenman, D. J.; Strodel, B.; Tarus, B.; Viles, J. H.; Zhang, T.; Wang, C.; Derreumaux, P. Amyloid β Protein and Alzheimer's Disease: When Computer Simulations Complement Experimental Studies. *Chemical Reviews* 2015, 115, 3518-3563.
26. Lin, Y.-S.; Bowman, G. R.; Beauchamp, Kyle A.; Pande, V. Investigating How Peptide Length and a Pathogenic Mutation Modify the Structural Ensemble of Amyloid Beta Monomer. *Biophysical Journal* 2012, 102, 315-324.
27. Ozbil, M.; Barman, A.; Bora, R. P.; Prabhakar, R. Computational Insights into Dynamics of Protein Aggregation and Enzyme–Substrate Interactions. *J. Phys. Chem. Lett.* 2012, 3, 3460-3469.
28. Côté, S.; Laghaei, R.; Derreumaux, P.; Mousseau, N. Distinct Dimerization for Various Alloforms of the Amyloid-Beta Protein: Aβ1–40, Aβ1–42, and Aβ1–40(D23N). *The Journal of Physical Chemistry B* 2012, 116, 4043-4055.
29. Gnanakaran, S.; Nussinov, R.; García, A. E. Atomic-Level Description of Amyloid beta-Dimer Formation. *J Am Chem Soc* 2006, 128, 2158-2159.
30. Urbanc, B.; Cruz, L.; Ding, F.; Sammond, D.; Khare, S.; Buldyrev, S. V.; Stanley, H. E.; Dokholyan, N. V. Molecular Dynamics Simulation of Amyloid beta Dimer Formation. *Biophysical journal* 2004, 87, 2310-2321.
31. Mitternacht, S.; Staneva, I.; Härd, T.; Irbäck, A. Monte Carlo study of the formation and conformational properties of dimers of Aβ42 variants. *J. Mol. Biol.* 2011, 410, 357-367.
32. Zhu, X.; Bora, R. P.; Barman, A.; Singh, R.; Prabhakar, R. Dimerization of the Full-Length Alzheimer Amyloid beta-Peptide (Abeta42) in Explicit Aqueous Solution: A Molecular Dynamics Study. *J Phys Chem B* 2012, 116, 4405-4416.
33. Jose, J. C.; Chatterjee, P.; Sengupta, N. Cross Dimerization of Amyloid-β and αSynuclein Proteins in Aqueous Environment: A Molecular Dynamics Simulations Study. *PLoS One* 2014, 9, e106883.
34. Tarus, B.; Tran, T. T.; Nasica-Labouze, J.; Sterpone, F.; Nguyen, P. H.; Derreumaux, P. Structures of the Alzheimer's Wild-Type Aβ1-40 Dimer from Atomistic Simulations. *The Journal of Physical Chemistry B* 2015, 119, 10478-10487.
35. Barz, B.; Olubiyi, O. O.; Strodel, B. Early amyloid [small beta]-protein aggregation precedes conformational change. *Chemical Communications* 2014, 50, 5373-5375.

36. Urbanc, B.; Betnel, M.; Cruz, L.; Bitan, G.; Teplow, D. B. Elucidation of Amyloid β-Protein Oligomerization Mechanisms: Discrete Molecular Dynamics Study. *Journal of the American Chemical Society* 2010, 132, 4266-4280.
37. Zheng, W.; Tsai, M.-Y.; Chen, M.; Wolynes, P. G. Exploring the aggregation free energy landscape of the amyloid-β protein (1–40). *Proceedings of the National Academy of Sciences* 2016.
38. Das, P.; Kang, S.-g.; Temple, S.; Belfort, G. Interaction of Amyloid Inhibitor Proteins with Amyloid Beta Peptides: Insight from Molecular Dynamics Simulations. *PLoS ONE* 2014, 9, e113041.
39. Sørensen, J.; Periole, X.; Skeby, K. K.; Marrink, S.-J.; Schiøtt, B. Protofibrillar Assembly Toward the Formation of Amyloid Fibrils. *J. Phys. Chem. Lett.* 2011, 2, 2385-2390.
40. Friedman, R.; Pellarin, R.; Caflisch, A. Soluble protofibrils as metastable intermediates in simulations of amyloid fibril degradation induced by lipid vesicles. *J. Phys. Chem. Lett.* 2009, 1, 471-474.
41. Baumketner, A.; Bernstein, S. L.; Wyttenbach, T.; Bitan, G.; Teplow, D. B.; Bowers, M. T.; Shea, J.-E. Amyloid β-protein monomer structure: A computational and experimental study. *Protein Science* 2006, 15, 420-428.
42. Tarus, B.; Straub, J. E.; Thirumalai, D. Dynamics of Asp23−Lys28 Salt-Bridge Formation in Aβ10-35 Monomers. *Journal of the American Chemical Society* 2006, 128, 16159-16168.
43. Fawzi, N. L.; Kohlstedt, K. L.; Okabe, Y.; Head-Gordon, T. Protofibril Assemblies of the Arctic, Dutch, and Flemish Mutants of the Alzheimer's Aβ(1–40) Peptide. *Biophys. J.* 2008, 94, 2007-2016.
44. Mitternacht, S.; Staneva, I.; Härd, T.; Irbäck, A. Monte Carlo study of the formation and conformational properties of dimers of Aβ42 variants. *Journal of molecular biology* 2011, 410, 357-367.
45. Barz, B.; Urbanc, B. Dimer Formation Enhances Structural Differences between Amyloid β-Protein (1–40) and (1–42): An Explicit-Solvent Molecular Dynamics Study. *PLoS ONE* 2012, 7, e34345.
46. Roche, J.; Shen, Y.; Lee, J. H.; Ying, J.; Bax, A. Monomeric Aβ1–40 and Aβ1–42 Peptides in Solution Adopt Very Similar Ramachandran Map Distributions That Closely Resemble Random Coil. *Biochemistry* 2016, 55, 762-775.
47. Kirkitadze, M. D.; Condron, M. M.; Teplow, D. B. Identification and characterization of key kinetic intermediates in amyloid β-protein fibrillogenesis1. *Journal of Molecular Biology* 2001, 312, 1103-1119.
48. Bitan, G.; Kirkitadze, M. D.; Lomakin, A.; Vollers, S. S.; Benedek, G. B.; Teplow, D. B. Amyloid beta-protein (Abeta) assembly: Abeta40 and Abeta42 oligomerize through distinct pathways. *Proceedings of the National Academy of Sciences* 2003, 100, 330-335.
49. O'Nuallain, B.; Freir, D. B.; Nicoll, A. J.; Risse, E.; Ferguson, N.; Herron, C. E.; Collinge, J.; Walsh, D. M. Amyloid β-Protein Dimers Rapidly Form Stable Synaptotoxic Protofibrils. *The Journal of Neuroscience* 2010, 30, 14411-14419.
50. Gu, L.; Liu, C.; Guo, Z. Structural insights into Aβ42 oligomers using site-directed spin labeling. *Journal of Biological Chemistry* 2013, 288, 18673-18683.
51. Tjernberg, L. O.; Näslund, J.; Lindqvist, F.; Johansson, J.; Karlström, A. R.; Thyberg, J.; Terenius, L.; Nordstedt, C. Arrest of-amyloid fibril formation by a pentapeptide ligand. *Journal of Biological Chemistry* 1996, 271, 8545-8548.

52. Kumari, R.; Kumar, R.; Lynn, A. g_mmpbsa—A GROMACS Tool for High-Throughput MM-PBSA Calculations. *Journal of Chemical Information and Modeling* 2014, 54, 1951-1962.
53. Marklund, Erik G.; Degiacomi, Matteo T.; Robinson, Carol V.; Baldwin, Andrew J.; Benesch, Justin L. P. Collision Cross Sections for Structural Proteomics. *Structure* 23, 791-799.
54. Pujol-Pina, R.; Vilaprinyó-Pascual, S.; Mazzucato, R.; Arcella, A.; Vilaseca, M.; Orozco, M.; Carulla, N. SDS-PAGE analysis of Aβ oligomers is disserving research into Alzheimer´s disease: appealing for ESI-IM-MS. *Scientific Reports* 2015, 5, 14809.
55. Yu, L.; Edalji, R.; Harlan, J. E.; Holzman, T. F.; Lopez, A. P.; Labkovsky, B.; Hillen, H.; Barghorn, S.; Ebert, U.; Richardson, P. L.; Miesbauer, L.; Solomon, L.; Bartley, D.; Walter, K.; Johnson, R. W.; Hajduk, P. J.; Olejniczak, E. T. Structural Characterization of a Soluble Amyloid β-Peptide Oligomer. *Biochemistry* 2009, 48, 1870-1877.
56. Hwang, W.; Zhang, S.; Kamm, R. D.; Karplus, M. Kinetic control of dimer structure formation in amyloid fibrillogenesis. *Proceedings of the National Academy of Sciences of the United States of America* 2004, 101, 12916-12921.
57. Cheon, M.; Chang, I.; Mohanty, S.; Luheshi, L. M.; Dobson, C. M.; Vendruscolo, M.; Favrin, G. Structural Reorganisation and Potential Toxicity of Oligomeric Species Formed during the Assembly of Amyloid Fibrils. *PLoS Computational Biology* 2007, 3, e173.
58. Qiao, Q.; Bowman, G. R.; Huang, X. Dynamics of an Intrinsically Disordered Protein Reveal Metastable Conformations That Potentially Seed Aggregation. *Journal of the American Chemical Society* 2013, 135, 16092-16101.
59. Rosenman, D. J.; Connors, C. R.; Chen, W.; Wang, C.; Garcia, A. E. Abeta Monomers Transiently Sample Oligomer and Fibril-Like Configurations: Ensemble Characterization Using a Combined MD/NMR Approach. *J Mol Biol* 2013, 425, 3338-3359.
60. Thirumalai, D.; Reddy, G.; Straub, J. E. Role of water in protein aggregation and amyloid polymorphism. *Accounts of chemical research* 2011, 45, 83-92.
61. Daidone, I.; Simona, F.; Roccatano, D.; Broglia, R. A.; Tiana, G.; Colombo, G.; Di Nola, A. β-Hairpin conformation of fibrillogenic peptides: Structure and α-β transition mechanism revealed by molecular dynamics simulations. *Proteins: Structure, Function, and Bioinformatics* 2004, 57, 198-204.
62. Meinhardt, J.; Tartaglia, G. G.; Pawar, A.; Christopeit, T.; Hortschansky, P.; Schroeckh, V.; Dobson, C. M.; Vendruscolo, M.; FÃ¤ndrich, M. Similarities in the thermodynamics and kinetics of aggregation of disease-related Abeta(1-40) peptides. *Protein science* 2007, 16, 1214-1222.
63. Lv, Z.; Roychaudhuri, R.; Condron, M. M.; Teplow, D. B.; Lyubchenko, Y. L. Mechanism of amyloid beta-protein dimerization determined using single-molecule AFM force spectroscopy. *Sci. Rep.* 2013, 3.
64. Schmidt, M.; Rohou, A.; Lasker, K.; Yadav, J. K.; Schiene-Fischer, C.; Fändrich, M.; Grigorieff, N. Peptide dimer structure in an Aβ(1–42) fibril visualized with cryo-EM. *Proc. Natl. Acad. Sci. U S A* 2015, 112, 11858-11863.
65. Ono, K.; Condron, M. M.; Teplow, D. B. Effects of the English (H6R) and Tottori (D7N) familial Alzheimer disease mutations on amyloid beta-protein assembly and toxicity. *Journal of Biological Chemistry* 2010, 285, 23186-23197.
66. Qahwash, I.; Weiland, K. L.; Lu, Y.; Sarver, R. W.; Kletzien, R. F.; Yan, R. Identification of a mutant amyloid peptide that predominantly forms neurotoxic protofibrillar aggregates. *Journal of Biological Chemistry* 2003, 278, 23187-23195.

67. Jawhar, S.; Wirths, O.; Bayer, T. A. Pyroglutamate Amyloid-beta (Abeta): A Hatchet Man in Alzheimer Disease. *Journal of Biological Chemistry* 2011, 286, 38825-38832.
68. Zago, W.; Buttini, M.; Comery, T. A.; Nishioka, C.; Gardai, S. J.; Seubert, P.; Games, D.; Bard, F. d. r.; Schenk, D.; Kinney, G. G. Neutralization of soluble, synaptotoxic amyloid beta species by antibodies is epitope specific. *The Journal of Neuroscience* 2012, 32, 2696-2702.
69. Li, H.; Du, Z.; Lopes, D. H. J.; Fradinger, E. A.; Wang, C.; Bitan, G. C-Terminal Tetrapeptides Inhibit Abeta42-Induced Neurotoxicity Primarily through Specific Interaction at the N-Terminus of Abeta42. *Journal of Medicinal Chemistry* 2014, 54, 8451-8460.
70. Diomede, L.; Romeo, M.; Cagnotto, A.; Rossi, A.; Beeg, M.; Stravalaci, M.; Tagliavini, F.; Di Fede, G.; Gobbi, M.; Salmona, M. The new β amyloid-derived peptide Aβ1–6 A2V-TAT (D) prevents Aβ oligomer formation and protects transgenic C. elegans from Aβ toxicity. *Neurobiology of Disease* 2016.
71. Ma, B.; Nussinov, R. Polymorphic Triple beta-Sheet Structures Contribute to Amide Hydrogen/Deuterium (H/D) Exchange Protection in the Alzheimer Amyloid beta42 Peptide. *Journal of Biological Chemistry* 2011, 286, 34244-34253.
72. Ball, K. A.; Phillips, A. H.; Wemmer, D. E.; Head-Gordon, T. Differences in beta-strand Populations of Monomeric A beta 40 and A beta 42. *Biophysical Journal* 2013, 104, 2714-2724.
73. Nguyen, P. H.; Sterpone, F.; Campanera, J. M.; Nasica-Labouze, J.; Derreumaux, P. Impact of the A2V mutation on the Heterozygous and Homozygous Aβ1-40 Dimer Structures from Atomistic Simulations. *ACS Chemical Neuroscience* 2016.
74. Kagan, B. L.; Jang, H.; Capone, R.; Arce, F. T.; Ramachandran, S.; Lal, R.; Nussinov, R. Antimicrobial Properties of Amyloid Peptides. *Molecular Pharmaceutics* 2012, 9, 708-717.
75. Bleiholder, C.; Do, T. D.; Wu, C.; Economou, N. J.; Bernstein, S. S.; Buratto, S. K.; Shea, J.-E.; Bowers, M. T. Ion Mobility Spectrometry Reveals the Mechanism of Amyloid Formation of Aβ (25–35) and Its Modulation by Inhibitors at the Molecular Level: Epigallocatechin Gallate and Scyllo-inositol. *Journal of the American Chemical Society* 2013, 135, 16926-16937.
76. Nie, Q.; Du, X.-g.; Geng, M.-y. Small molecule inhibitors of amyloid [beta] peptide aggregation as a potential therapeutic strategy for Alzheimer's disease. *Acta Pharmacol Sin* 2011, 32, 545-551.
77. Gessel, M. M.; Wu, C.; Li, H.; Bitan, G.; Shea, J.-E.; Bowers, M. T. Aβ (39–42) modulates Aβ oligomerization but not fibril formation. *Biochemistry* 2011, 51, 108-117.
78. Esteras-Chopo, A.; Morra, G.; Moroni, E.; Serrano, L.; Lopez de la Paz, M.; Colombo, G. A molecular dynamics study of the interaction of D-peptide amyloid inhibitors with their target sequence reveals a potential inhibitory pharmacophore conformation. *Journal of molecular biology* 2008, 383, 266-280.
79. Wilhelmus, M. M. M.; Otte-Höller, I.; Wesseling, P.; De Waal, R. M. W.; Boelens, W. C.; Verbeek, M. M. Specific association of small heat shock proteins with the pathological hallmarks of Alzheimer's disease brains. *Neuropath Appl Neuro* 2006, 32, 119-130.
80. Luo, J.; Warmlander, S. K. T. S.; Graslund, A.; Abrahams, J. P. Human lysozyme inhibits the in vitro aggregation of Abeta peptides, which in vivo are associated with Alzheimer's disease. *Chem Comm* 2013, 49, 6507-6509.
81. Sugita, Y.; Okamoto, Y. Replica-exchange molecular dynamics method for protein folding. *Chemical Physics Letters* 1999, 314, 141-151.
82. Miyashita, N.; Straub, J. E.; Thirumalai, D. Structures of beta-Amyloid Peptide 1-40, 1-42, and 1-55-the 672-726 Fragment of APP-in a Membrane Environment with Implications for

Interactions with gamma-Secretase. *Journal of the American Chemical Society* 2009, 131, 17843-17852.
83. Sgourakis, N. G.; Merced-Serrano, M.; Boutsidis, C.; Drineas, P.; Du, Z.; Wang, C.; Garcia, A. E. Atomic-level characterization of the ensemble of the Aβ(1-42) monomer in water using unbiased Molecular Dynamics simulations and spectral algorithms. *J. Mol. Biol.* 2011, 405, 570-583.
84. Fukunishi, H.; Watanabe, O.; Takada, S. On the Hamiltonian replica exchange method for efficient sampling of biomolecular systems: Application to protein structure prediction. *J. Chem. Phys.* 2002, 116, 9058-9067.
85. Patriksson, A.; van der Spoel, D. A temperature predictor for parallel tempering simulations. *Physical Chemistry Chemical Physics* 2008, 10, 2073-2077.
86. Deserno, M.; Holm, C. How to mesh up Ewald sums. II. An accurate error estimate for the particle–particle–particle-mesh algorithm. *Journal of Chemical Physics* 1998, 109, 7694-7701.
87. Hess, B.; Bekker, H.; Berendsen, H. J. C.; Fraaije, J. G. E. M. LINCS: A linear constraint solver for molecular simulations. *Journal of Computational Chemistry* 1997, 18, 1463-1472.
88. Miyamoto, S.; Kollman, P. A. Settle: An analytical version of the SHAKE and RATTLE algorithm for rigid water models. *Journal of Computational Chemistry* 1992, 13, 952-962.
89. Hess, B.; Kutzner, C.; Van Der Spoel, D.; Lindahl, E. GROMACS 4: Algorithms for highly efficient, load-balanced, and scalable molecular simulation. *Journal of Chemical Theory and Computation* 2008, 4, 435-447.
90. Jorgensen, W. L.; Maxwell, D.; Tirado-Rives, J. Development and testing of the OPLS all-atom force field on confromational energetics and properties of organic liquids. *J. Am. Chem. Soc.* 1996, 118, 11225-11236.
91. Jorgensen, W. L.; Chandrasekhar, J.; Madura, J. D.; Impey, R. W.; Klein, M. L. Comparison of simple potential functions for simulating liquid water. *J Chem Phys* 1983, 79, 926-935.
92. Nguyen, P. H.; Li, M. S.; Derreumaux, P. Effects of all-atom force fields on amyloid oligomerization: replica exchange molecular dynamics simulations of the A[small beta]16-22 dimer and trimer. *Physical Chemistry Chemical Physics* 2011, 13, 9778-9788.
93. Frishman, D.; Argos, P. Knowledge-based protein secondary structure assignment. *Proteins* 1995, 23, 566-579.
94. Aronovitz, J.; Nelson, D. Universal features of polymer shapes. *Journal de physique* 1986, 47, 1445-1456.
95. Humphrey, W.; Dalke, A.; Schulten, K. VMD: visual molecular dynamics. *Journal of molecular graphics* 1996, 14, 33-38.
96. Baker, N. A.; Sept, D.; Joseph, S.; Holst, M. J.; McCammon, J. A. Electrostatics of nanosystems: Application to microtubules and the ribosome. *Proceedings of the National Academy of Sciences* 2001, 98, 10037-10041.
97. Daura, X.; Gademann, K.; Jaun, B.; Seebach, D.; van Gunsteren, W. F.; Mark, A. E. Peptide Folding: When Simulation Meets Experiment. *Angewandte Chemie International Edition* 1999, 38, 236-240.
98. Bohrer, B. C.; Merenbloom, S. I.; Koeniger, S. L.; Hilderbrand, A. E.; Clemmer, D. E. Biomolecule analysis by ion mobility spectrometry. *Annual review of analytical chemistry (Palo Alto, Calif.)* 2008, 1, 293-327.

Table 1: Summary of WT+A2T Aβ_{42} experiment and simulation results.

Simulation findings	**WT Aβ_{42} homodimer**	**A2T Aβ_{42} heterodimer**
Average radius of gyration (in nm)	1.28	1.28
$\Delta G_{Binding}$ (kcal/mol)	-17.8	-43.4
Overall Secondary structure	Reference	Stronger β-strand propensity at NTR
CHC-CTR tertiary contact probability*	0.21	0.12
Population (in %) of disordered structures with a weak interface (S1 state)	9.4	22.7
Population (in %) of structures with a strong, β-sheet rich interface (S2 state)	20.7	15.8
Population (in %) of hairpin structures with a weak interface (S4 state)	22.4	13.2
Experimental observations	**WT Aβ_{42}**	**1:1 WT+A2T Aβ_{42}**
Aggregation kinetics (ThT fluorescence) [7]	Reference[#]	No difference
Aggregation (ThT fluorescence) [8]	Reference[#]	Lower level and slower kinetics
AFM after 2h of aggregation [7]	Reference[#]	Smaller aggregate
ANS binding emission peak (nm) [7]	502	512
ANS binding relative peak magnitude (in a.u.) [7]	1	0.77
FTIR peak locations (cm^{-1}) [7]	1627, 1650, 1685	1627, 1657, 1665
Arrival time distributions of the z/n = −5/2 (IM-MS) [11]	Formation of dimer, tetramer, hexamer, and dodecamer	Dimer, tetramer, hexamer, but no dodecamer

[#] Implies that WT Aβ_{42} dimer data has been used as a reference for comparison.

*Defined as $\langle Q_{ij} \rangle_{i=15\text{-}21,\, j=29\text{-}42}$, Q=contact probability. Only those contacts were considered, for which (Q_{ij}^{homo} - Q_{ij}^{hetero}) was greater than 0.05.

FIGURES

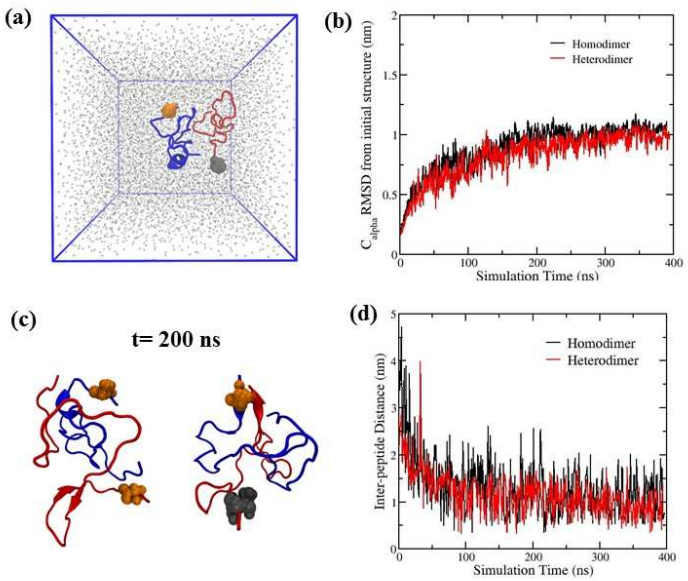

Figure 1. (a) Initial structure of the two peptide system in a water box for A2T heterodimer. Peptide chains (displayed using cartoon representation) are colored in blue and red. Residue 2 is represented as van der Waals spheres (orange for A2 and grey for T2). Water is shown in blue. **(b)** Root-mean-square distance (RMSD), in nm, from the initial peptide structure (C_α atoms only considered), averaged over two chains, as a function of simulation time for the 310 K trajectory (homodimer in black and heterodimer in red). **(c)** Snapshot of the system at 200 ns (homodimer on left and heterodimer on right). Color scheme used is same as in Fig. 1a. **(d)** Evolution of the distance between the center of mass (COM) of two chains at 310 K (homodimer in black and heterodimer in red).

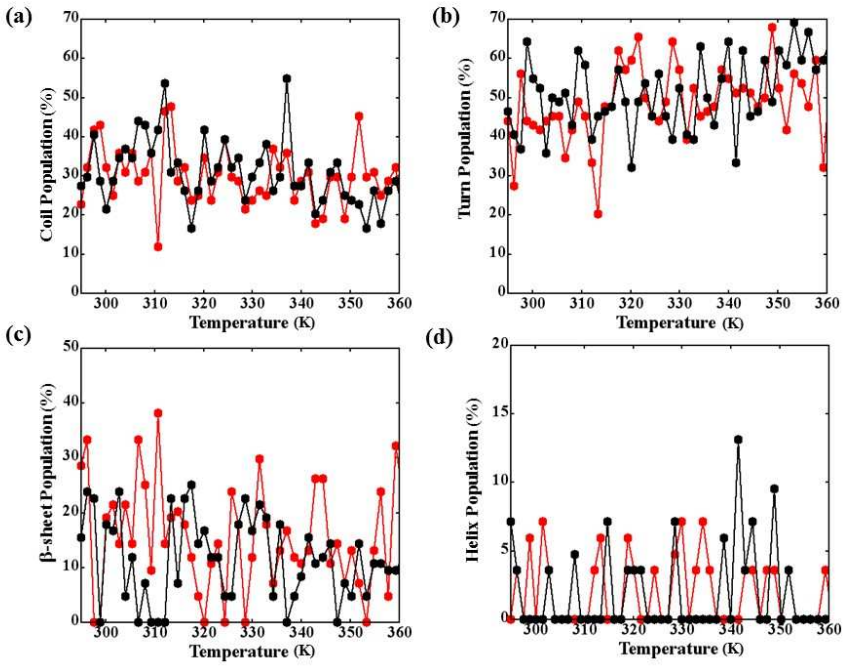

Figure 2. (a-d) Percentage population of secondary structural elements, averaged over two chains, at 200 ns for replicas spanning 295-360 K temperature range: (a) coil, (b) turn, (c) β-sheet, and (d) α-helix. Results for homodimer system are shown in black and for heterodimer system are shown in red.

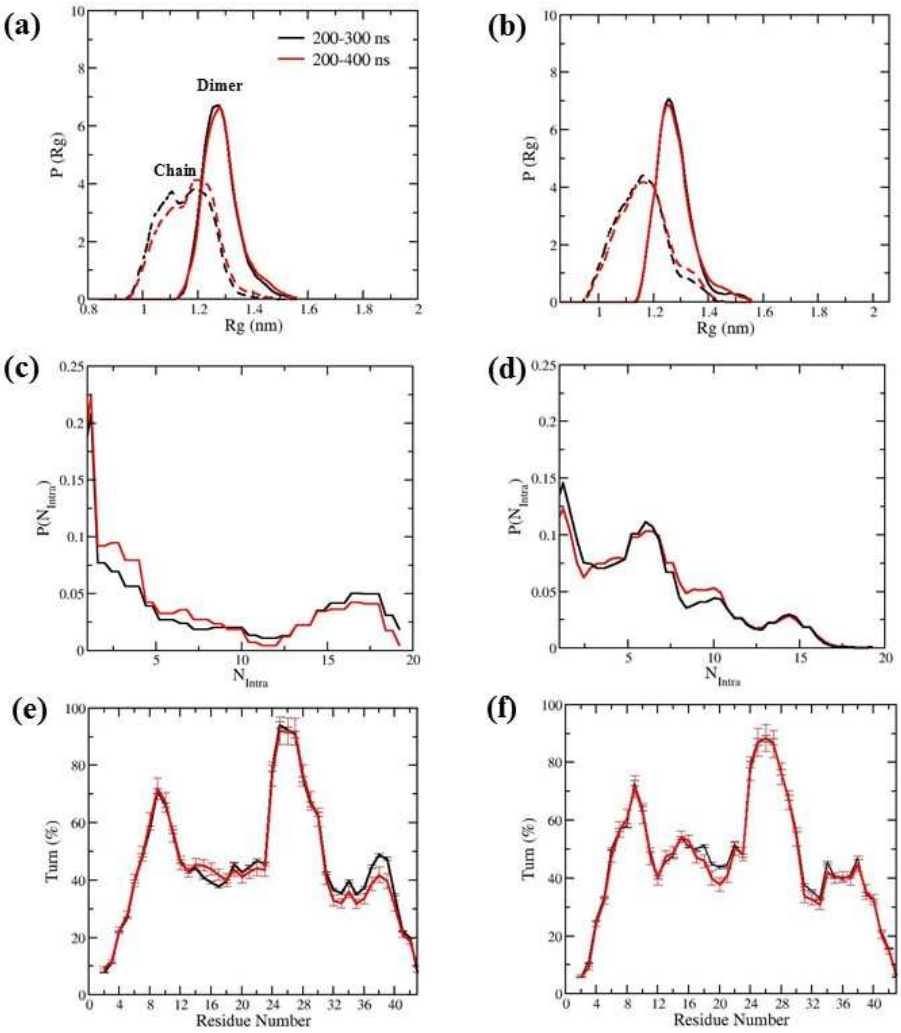

Figure 3. REMD convergence analysis. Probability distributions of **(a-b)** radius of gyration, Rg, (in nm, solid line: dimer, dashed line: individual chain), of **(c-d)** number of intra-chain contacts (C_α atoms only), N_{intra}, and **(e-f)** residue-wise turn propensity (in %) estimated from sampling obtained during 200-300 ns (black) and during 200-400 ns (red) at 310 K. Standard errors are obtained from standard deviations estimated by dividing data in smaller two or four 50 ns long blocks. Results for homodimer are shown in left panel and for heterodimer are shown in right panel.

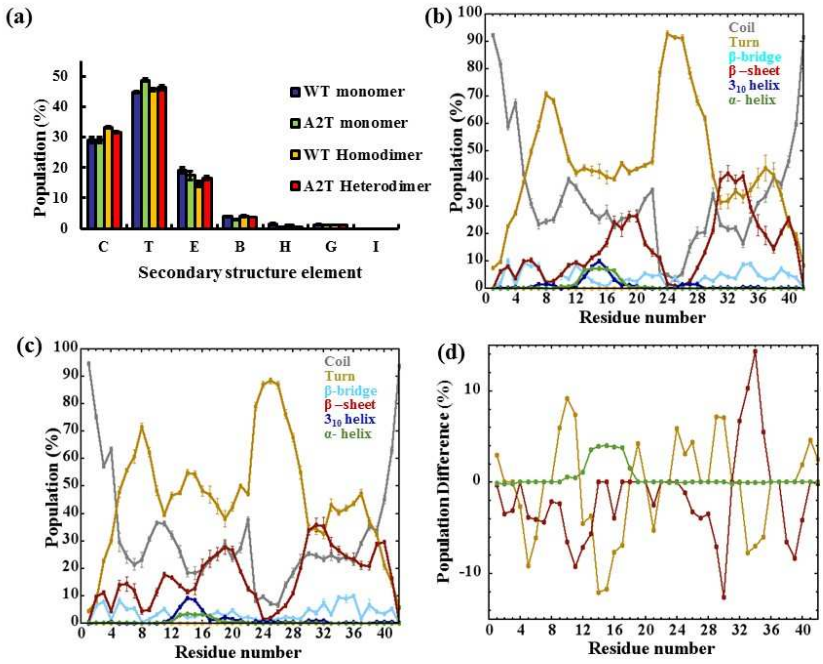

Figure 4. Secondary structure analysis. **(a)** Overall population (in %) of secondary structural elements (C=coil, T=Turn, E=β-strand, B=β-bridge, H=α-helix, G=3_{10}-helix, I=π-helix). The standard errors were estimated by splitting the 200 ns data in four 50 ns long segments and computing the standard deviations of the averages of those 50 ns long segments. Secondary structural propensities for the WT and A2T monomeric ensembles are taken from ref. [13]. **(b-c)** Secondary structure per residue for **(b)** WT homodimer, and **(c)** A2T heterodimer. Color-scheme used is as follows: Coil = gray, Turn = gold, β-bridge = cyan, β-strand = red, 3_{10}-helix = blue, α-helix = green**. (d)** α-helix, β-strand, and turn population differences (in %) between homo- and hetero-dimeric system. Positive values indicate higher propensity in homodimer. Color-scheme used is same as in (b).

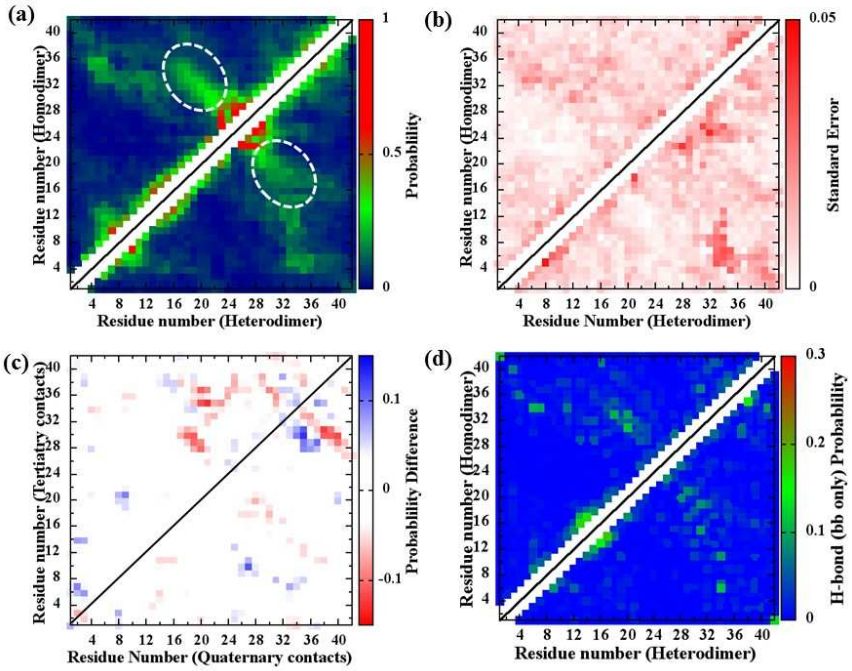

Figure 5. Tertiary structure analysis. (a) Ensemble-averaged intra-molecular Cα contact maps for WT homo- (upper triangle) and A2T hetero- (lower triangle) dimer systems. Non-sequential contacts, i.e.|i-j| ≥3, are only shown. White dotted circle highlights the CHC-CTR anti-diagonal contacts. **(b)** Standard errors associated with tertiary contact probability calculation for homodimer (upper triangle) and heterodimer (lower triangle). **(c)** Arithmetic difference between the contact probabilities of homodimer and heterodimer (upper and lower triangle corresponds to tertiary and quaternary contacts, respectively). **(d)** Ensemble-averaged probabilities of H-bonding (backbone only) formation (upper triangle = homodimer, lower triangle = heterodimer). Color-scale used is shown on the right of the corresponding figure.

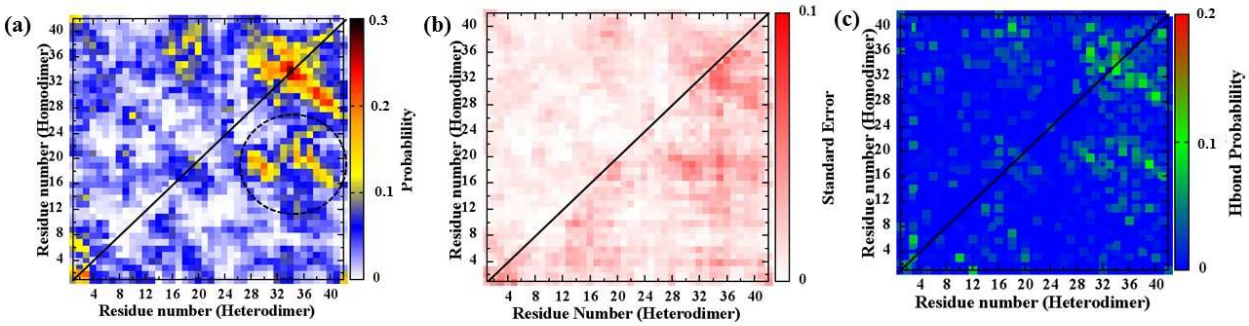

Figure 6. Quaternary structure analysis. (a) Inter-chain contact maps (heavy atoms only), **(b)** standard errors for quaternary contact probabilities, and **(c)** inter-chain H-bonding (backbone only) probabilities for WT homodimer (upper triangle) and A2T heterodimer (lower triangle). The color-scheme used in each case is also shown. Black dotted circle in (a) highlights stronger presence of CHC-CTR inter-chain contacts in heterodimer.

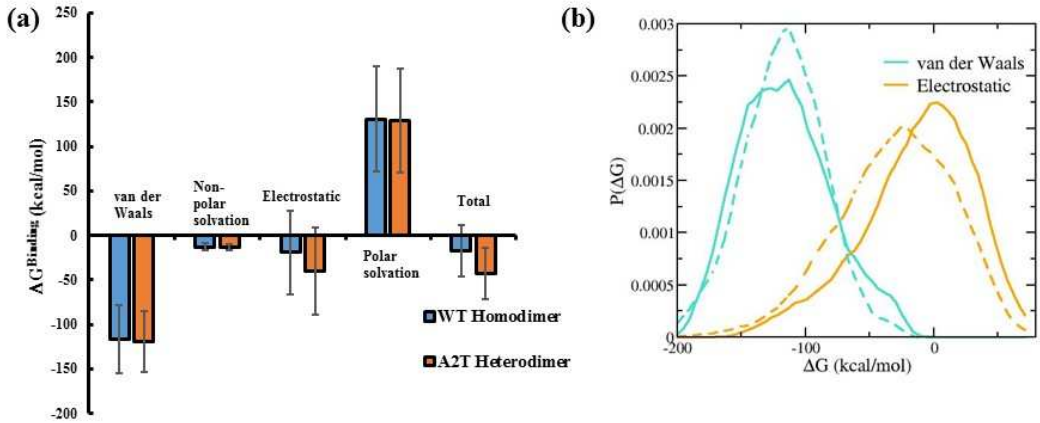

Figure 7. Inter-chain Binding Free Energy Estimation: (a) Contributions of the individual energy components and total free energy of binding (in kcal/mol). **(b-c)** Energy distributions, (b) vdW and (c) electrostatics (solid line: homodimer, dashed line: heterodimer).

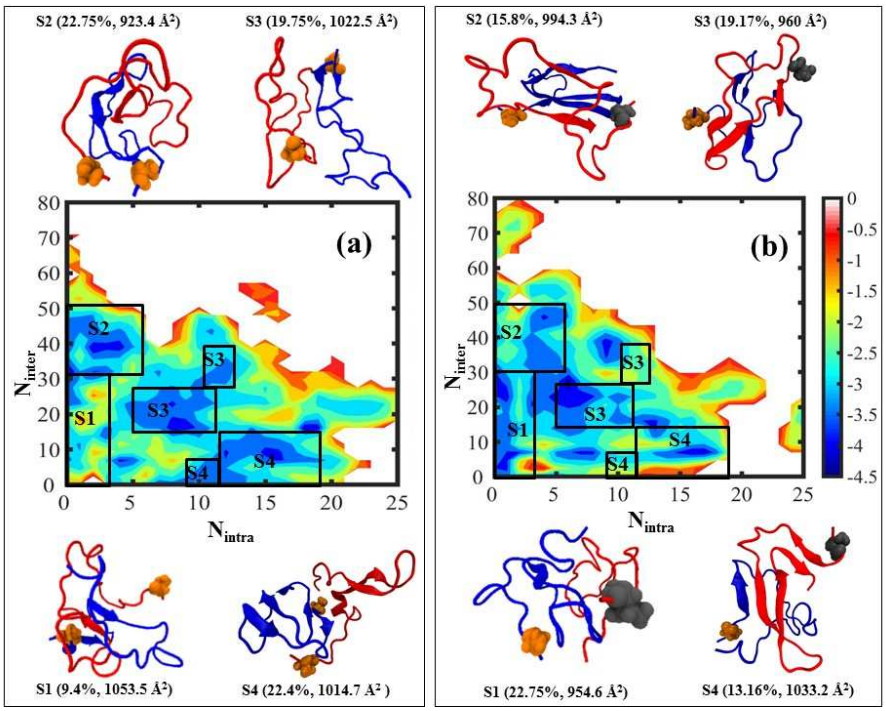

Figure 8. Dimeric Conformational Landscapes: 2D Potential of Mean Force (PMF) plots as a function of number of intra- (N_{intra}) and inter-chain (N_{intra}) contacts of **(a)** WT homo- and **(b)** A2T heterodimer (see Methods). The reported number of intra-chain contacts is estimated by averaging over two chains. Each contour level represents 0.5 kcal/mol. Black squares denote the discrete regions (S1-S4) on the PMF plots, which individually represents ≥9% of the WT dimer production ensemble. The representative conformation of the largest cluster for each of those regions is shown using cartoon representation. Color scheme used for individual peptides used is same as in Figure 1. Also shown are the % population of individual states (S1-S4) and the collision cross sectional area (CCS) of the representative conformations (in $Å^2$) in parenthesis.

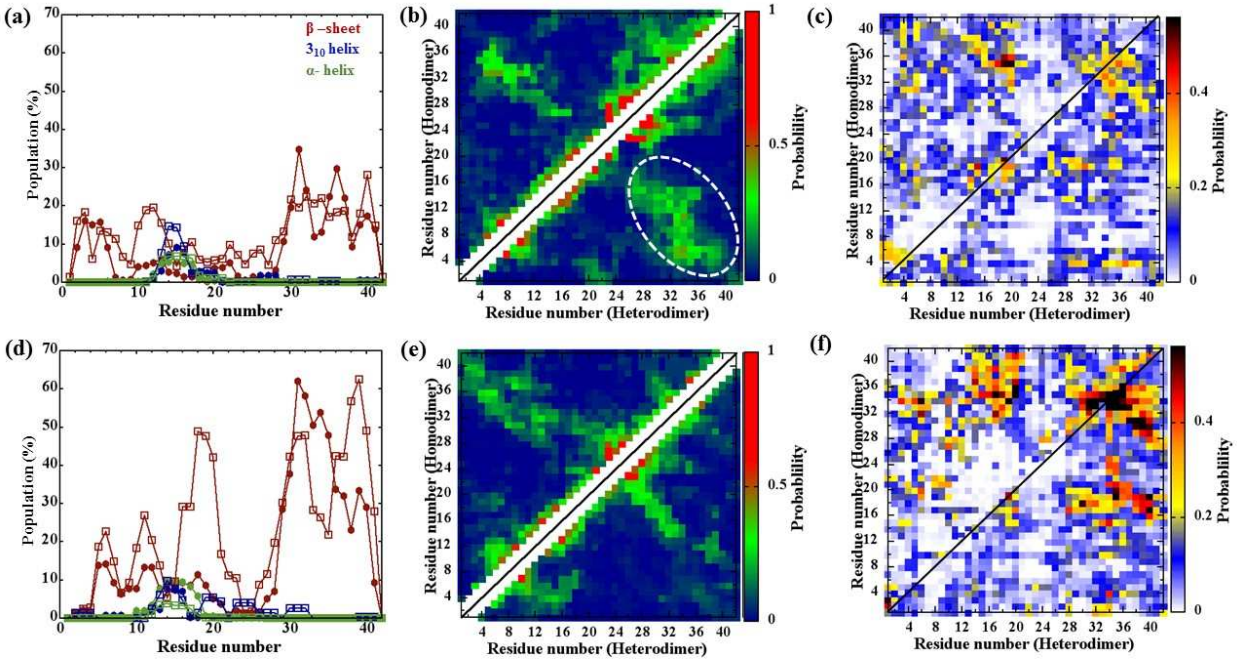

Figure 9. Structural analysis of S1 and S2 dimers. Top panel corresponds to S1 dimer and bottom panel represents S2 dimer. **(a & d)** Secondary structure per residue (filled circle = homodimer, empty square = heterodimer); **(b & e)** tertiary contact maps; and **(c & f)** inter-peptide contact maps. Color schemes used are same as Figure 4-6. White circle in (b) denotes presence of NTR-CTR tertiary contacts in S1 heterodimers.

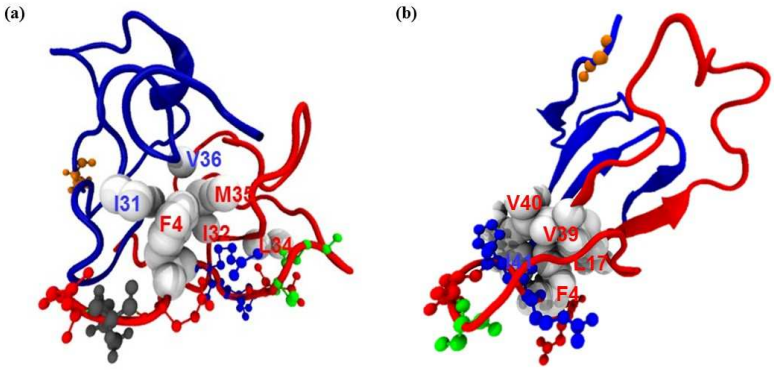

Figure 10. Representative S1 and S2 heterodimer structure. (a) A hydrophobic cluster in the S1 heterodimer consisting of F4, I32, and M35 from the A2T peptide and residues I31 and V36 from the WT peptide (shown in van der Waals spheres). The A2T N-terminus is shown in CPK representation (white = non-polar, green = polar, acidic = red, and basic = blue). (b) A2T NTR interacting with CHC and CTR hydrophobic residues that constitute a parallel β-sheet rich inter-chain interface in S2 heterodimer. Color scheme for individual peptides used is same as in Figure 1.

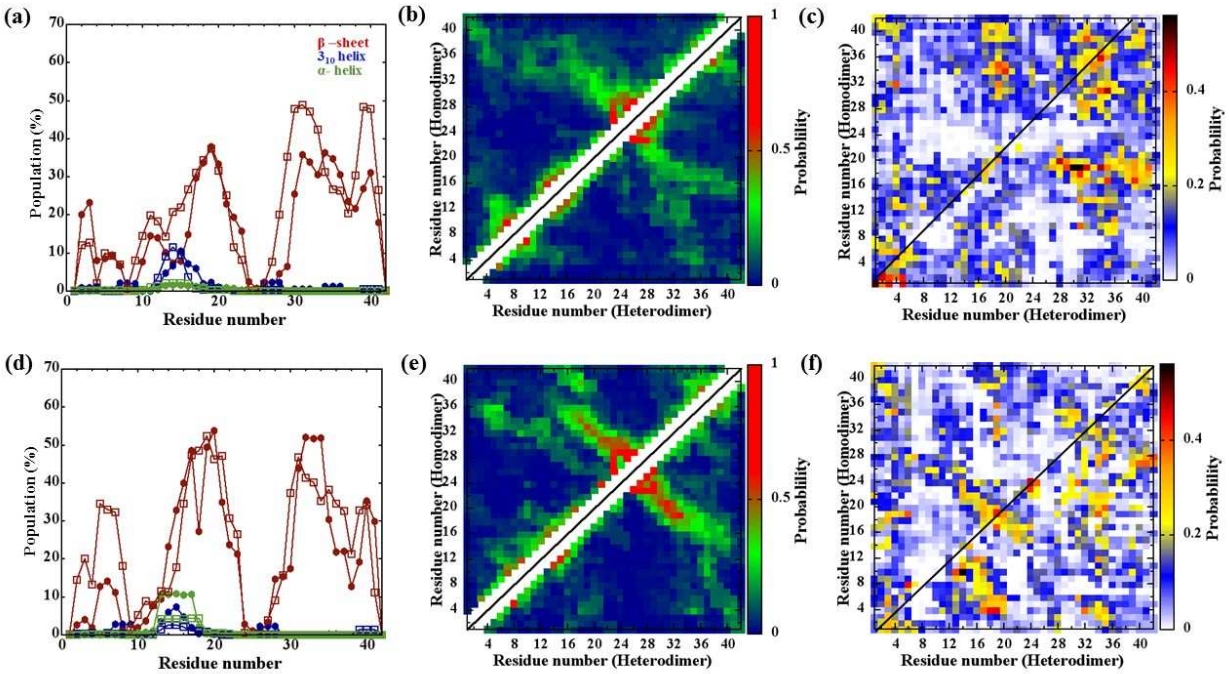

Figure 11. Structural analysis of S3 and S4 dimers. Top panel corresponds to S3 structures and bottom panel represents S4 structures. **(a & d)** Secondary structure per residue (filled circle = homodimer, empty square = heterodimer); **(b & e)** tertiary contact maps; and **(c & f)** inter-peptide contact maps. Color schemes used are same as Figures 4-6.

TOC Graphics